Carbohydrate Polymers 98 (2013) 1573–1577

Contents lists available at ScienceDirect

Carbohydrate Polymers

journal homepage: www.elsevier.com/locate/carbpol

Properties of novel polyvinyl alcohol/cellulose nanocrystals/silver nanoparticles blend membranes

Xu Xu[a,c], Yi-Qin Yang[b], Ying-Ying Xing[a,c], Jiu-Fang Yang[a,c], Shi-Fa Wang[a,c,*]

[a] Institute of Chemical Engineering, Nanjing Forestry University, Nanjing, Jiangsu 210037, People's Republic of China
[b] Institute of Light Industry Science and Engineering, Nanjing Forestry University, Nanjing, Jiangsu 210037, People's Republic of China
[c] Jiangsu Key Lab of Biomass-based green Fuels and Chemicals, Nanjing 210037, People's Republic of China

ARTICLE INFO

Article history:
Received 31 May 2013
Received in revised form 30 June 2013
Accepted 26 July 2013
Available online 7 August 2013

Keywords:
Cellulose nanocrystals
Silver nanoparticles
Polyvinyl alcohol
Nanocomposite

ABSTRACT

Novel polyvinyl alcohol (PVA) blend membranes containing cellulose nanocrystals (CNs) and silver nanoparticles (AgNPs) were prepared via a simple method. CNs were prepared by sulfuric acid treatment of microcrystalline cellulose. $AgNO_3$ aqueous solution mixed with the CNs aqueous suspension and was reduced by $NaBH_4$ at room temperature. Purified CNs/AgNPs nanocomposites as functional fillers mixed with polyvinyl alcohol to prepare blend membrane. The morphology, mechanical properties, and antibacterial activities of PVA/CNs/AgNPs composite films were investigated. The PVA/CNs/AgNPs composite films were stable and homogeneous. The tensile strength of PVA was increased from 57.02 MPa to 81.21 MPa when filled with CNs/AgNPs. Antibacterial ratio of PVA/CNs/AgNPs composite against Gram-negative *Escherichia coli* and Gram-positive *Staphylococcus aureus* was 96.9% and 88.2%, respectively. The CNs/AgNPs nanocomposites could be applied as bi-functional nanofillers within PVA to improve the mechanical properties and antibacterial activities.

1. Introduction

Cellulose is the most abundant and renewable carbon resource on the earth. As one of the most common organic polymers, cellulose is considered as an almost inexhaustible source of raw material for the increasing demand for making environmentally friendly and biocompatible products (Habibi, Lucia, & Rojas, 2010; Klemm, Heublein, Fink, & Bohn, 2005; Nathalie, Isabelle, Alain, & Julien, 2012). Cellulose nanocrystals (CNs) are rod-like defect free crystalline nanoparticles obtained after the acid hydrolysis of cellulose fibers (Anglès & Dufresne, 2011; Chen, Lawton, Thompson, & Liu, 2012; Habibi et al., 2010; Klemm et al., 2005), and they have special advantages including, easy modification, abundantly available, high surface areas, unique morphology, low density, and low thermal-expansion mechanical strength because of their nanoscale dimensions (Eichhorn, Young, & Davies, 2005; Fortunati et al., 2012; Khan et al., 2012; Brinchi, Cotana, Fortunati, & Kenny, 2013; Parisa, Tae, Karl, Rina, & Hamid, 2013). These characteristics make cellulose nanocrystals suitable as nanofiller for some polymer materials (Habibi et al., 2010).

Previous studies showed that large surface area of these nanofillers promotes better interfacial interactions with the polymer matrix compared to conventional micrometer size particles. Because of their interesting and useful characteristics, such as good mechanical properties, thermal resistance and chemical reagent resistance, researches on utilizing nanocellulose as filler in polymer matrices have increased significantly over the years (Cao, Habibi, & Lucia, 2009; Clemons et al., 2013; De Menezes, Siqueira, Curvelo, & Dufresne, 2009; Habibi & Dufresne, 2008; Liu, Cui, Shang, Wang, & Song, 2013; Ten, Jiang, & Wolcott, 2013). The major driving force for this type of research is its potential of exploiting the high stiffness of cellulose crystals. As one of important functional fillers, inorganic nanoparticle can provide new functionalities to the host polymer materials (Allen et al., 2004; Althues, Henle, & Kaskel, 2007; Bönnemann & Richards, 2011; Varga, Feher, Filipcsei, & Zrinyi, 2003). However, the formation of aggregates or agglomerates will greatly reduce applicability of inorganic nanoparticles. How to prepare inorganic nanoparticles without aggregation during their integration into the host polymer is a big challenge. In recent years, CNs as the carrier are being used to prepare CNs/inorganic nanoparticle complexes, as well as CNs composites have been widely studied (Shin, Bae, Arey, & Exarhos, 2008; Shinsuke, Manami, Minoru, Hiroyuki, & Hiroyuki, 2009; Liu, Wang, Shang, & Song, 2011). Polyvinyl alcohol (PVA) is an important water soluble polymer, and it has been widely used in medicine, construction, wood processing, paper making, printing, agriculture, polymer chemical industry because of its excellent film

* Corresponding author at: Institute of Chemical Engineering, Nanjing Forestry University, Nanjing, Jiangsu 210037, People's Republic of China.
Tel.: +86 25 85427812; fax: +86 25 85427812.
E-mail address: wangshifa65@163.com (S.-F. Wang).

0144-8617/$ – see front matter © 2013 Elsevier Ltd. All rights reserved.
http://dx.doi.org/10.1016/j.carbpol.2013.07.065

forming, emulsifying and adhesive properties. The improvement of PVA's mechanical and antimicrobial properties is valuable.

In this study, nanocomposites composed of cellulose nanocrystals (CNs) and silver nanoparticles (AgNPs) were prepared and incorporated into polyvinyl alcohol (PVA) as nanofillers. CNs was used as scaffolds and carriers for the stabilization of silver cations and AgNPs. AgNPs exhibit excellent antimicrobial properties and, therefore, the incorporation of the CNs/AgNPs nanocomposites as bifunctional fillers in PVA is expected to improve mechanical and antimicrobial properties of PVA. PVA-based composites were prepared by casting and evaporating mixtures of CNs/AgNPs and aqueous PVA suspensions in Teflon molds. The morphology, structure, and performance of the CNs/AgNPs nanocomposites and PVA-based composite films were investigated and characterized.

2. Experimental

2.1. Materials

Silver nitrate ($AgNO_3$), sulfuric acid (H_2SO_4, 98 wt%), sodium borohydride ($NaBH_4$), microcrystalline cellulose, ethanol (C_2H_5OH), phosphotungstic acid hydrate ($H_3O_{40}PW_{12}{\cdot}H_2O$), PVA (Mw: 1750) and sodium hydroxide (NaOH) were purchased from Sinopharm Chemical Reagent Co., Ltd. and used without further purification.

2.2. Preparation of cellulose nanocrystals

Cellulose nanocrystal powder was prepared by the acid-catalyzed hydrolysis of microcrystalline cellulose as previously described (Liu et al., 2011). Microcrystalline cellulose (6 g) was mixed with sulfuric acid solution (90 mL, 64 wt%) and the mixture was stirred vigorously at 40 °C for 2 h. The suspension was then diluted ten times to stop the reaction. The suspension of pH 2 was obtained by centrifuging and washing the CNs suspension with water repeatedly. Dialysis was performed to remove free acid in the suspension, and the result was monitored by checking the neutrality of the dialysis effluent. CNs powder was finally obtained through freeze-drying.

2.3. Preparation of CNs/AgNPs nanocomposites

CNs/AgNPs nanocomposites were prepared from the CNs suspension by the reduction of silver cation. In a typical preparation, 1 mL of aqueous $AgNO_3$ (1.0×10^{-2} M) was added to the suspension (30 g, 1 wt%), followed by 1 h of stirring, CNs/AgNPs gels were prepared by treating the suspension with 1 mL of $NaBH_4$ (1.0×10^{-2} M) solution at room temperature. After stirring for another 1 h, CNs/AgNPs nanocomposites were then phase-separated from the suspension by centrifugation at 10 000 × g. Under these conditions, CNs-based nanocomposites containing 0.36 wt% silver were prepared. Nanocomposites contained 1.77 wt% (5 mL, $AgNO_3$), 3.47 wt% (10 mL, $AgNO_3$), and 6.71 wt% (20 mL, $AgNO_3$) silver were also prepared under similar conditions.

2.4. Preparation of PVA and PVA/CNs/AgNPs nanocomposite films

The 10% PVA solution was prepared by dissolving of PVA in 100 mL distilled water at 90 °C for 4 h. The PVA solution was mixed with a specific amount of aqueous CNs and CNs/AgNPs dispersion and sonicated for 20 min. to obtain suspensions of different compositions. Resulting mixtures were stirred in a rotary evaporator under vacuum for 15 min to remove residual air and avoid the formation of irreversible bubbles during evaporation. Resulting mixtures were subsequently casted in Teflon molds and water was removed by atmospheric evaporation at room temperature. The dry composite films were roasted at 50 °C for 5 h. A series of nanocomposite films with a thickness of ~0.3 mm were prepared by altering the CNs content of 5 wt%, and are denoted as PVA/CNs. CNs/AgNPs nanocomposites with differing silver contents were mixed with PVA solutions for preparing composite films which are denoted as PVA/CNs/AgNPs-0.36, PVA/CNs/AgNPs-1.77, PVA/CNs/AgNPs-3.47, and PVA/CNs/AgNPs-6.71. The numerical value of Ag content in CNs/AgNPs was calculated by the filling amount of $AgNO_3$ and CNs. PVA film without filling any substance are denoted as PVA. Prior to characterization, the resulting films were conditioned at room temperature in a desiccator containing P_2O_5 with 0% relative humidity (RH).

2.5. Characterizations

The morphology of CNs and AgNPs was observed by transmission electron microscopy (TEM), using a JEOL 2100 microscope operating at 200 kV. TEM samples were typically prepared by dropping the sample suspension on a Cu grid coated with a carbon film, and TEM images of CNs were obtained by staining using 1.0 wt% phosphotungstic acid. Phosphotungstic acid hydrate was used as a negative staining agent for the TEM characterization of cellulose nanocrystal. The neat PVA film, PVA/CNs/AgNPs composite film, and a suspension of CNs/AgNPs were optically characterized using a Shimadzu 2550 UV-Vis spectrophotometer. The mechanical properties of the PVA-based films were measured on a universal testing machine (CMT 6503, Shenzhen SANS Test Machine Co. Ltd., China) and an average value of at least five replicates for each sample was taken. The X-ray diffractometry (XRD) (model WI-RES-XRD-001, Philips analytical, The Netherlands) was also employed to study PVA-based films. The X-ray source had a 40 kV operating voltage, 45 mA current, 10–80° angular (2θ), and a stepped angle of 0.2° (2θ)/s. Antibacterial activity testing of PVA-based films was adopted from ASTM G 21–09 and previously reported studies (Ma & Zhang, 2009; Kumar, Vemula, Ajayan, & John, 2008). Gram-negative *E. coli* and Gram positive *S. aureus* were selected for bactericidal testing.

3. Result and discussion

3.1. Morphology of CNs and AgNPs

The TEM image of CNs deposited from a dilute suspension is shown in Fig. 1, from which it is apparent the suspension contains cellulose fragments. Fragments appear as slender rods of 20 nm in diameter and 200 nm in length.

CNs' strong ability to adsorb metallic cations is attributed to its abundant surface hydroxyl groups. Hydroxyl groups result in the high density immobilization of silver nanoparticles on CNs because of their good adsorption of Ag^+ and Ag^0 (Shinsuke et al., 2009). CNs/AgNPs suspensions redispersed in distilled water are found to be stable, with no obvious deposition or flocculation observed within 4 months. TEM images of AgNPs are listed in Fig. 2, which show that nanostructures are formed in the CNs suspension, and AgNPs are dispersed in the presence of CNs. Average size of nanoparticles clearly increases with metal cation concentration (from 0.36 to 6.71%) during the synthesis. TEM characterization of nanocomposites shows well-contrasted AgNPs because CNs give little contrast against the resin (Cai, Kimura, Wada, & Kuga, 2009).

3.2. XRD and UV–vis characterization of PVA/CNs/AgNPS composite

The XRD patterns of CNs, CNs/AgNPs film and PVA/CNs/AgNPs film are shown in Fig. 3. The diffraction pattern of CNs exhibited the typical diffraction peaks of cellulose I at $2\theta = 16°$, 22.4°, and 34.3° respectively (Fig. 3a). The diffraction pattern of CNs/AgNPs

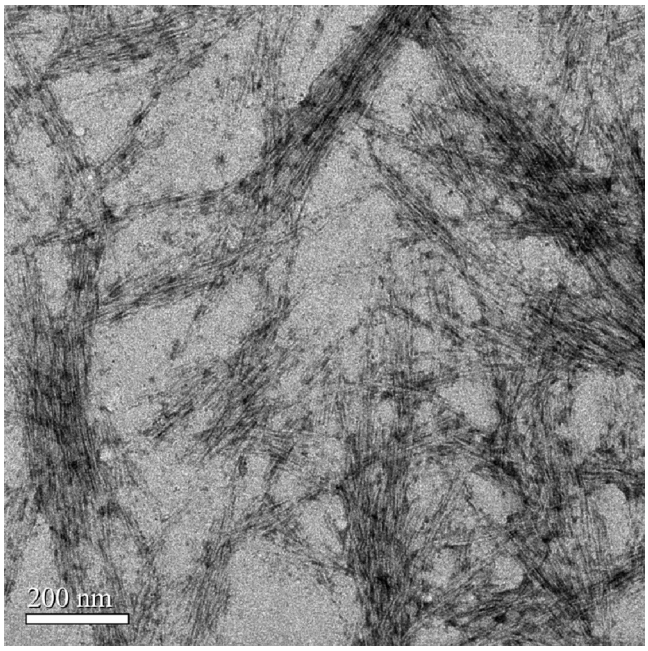

Fig. 1. TEM image of CNs.

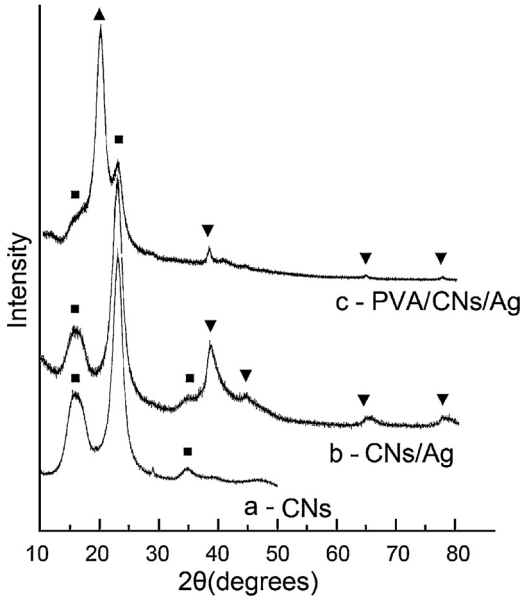

Fig. 3. XRD pattern of (a) CNs, (b) CNs/AgNPs nanocomposite, and (c) PVA/CNs/AgNPs film.

film showed four peaks at $2\theta = 38.1^\circ$, 44.19°, 64.4° and 77.4°, which were assigned to the (1 1 1), (2 0 0), (2 2 0) and (3 1 1) planes of Ag crystalline form (Fig. 3b). The diffraction pattern of PVA/CNs/AgNPs-3.47 blended film appeared one peak at $2\theta = 19.5^\circ$ (Fig. 3c), due to its crystallinity of PVA in the blended film. Moreover, the absence of other peaks in Fig. 4c can be attributed to the CNs and AgNPs, which indicated that the diffraction pattern of PVA/CNs/AgNPs membrane is the superposition of three substances.

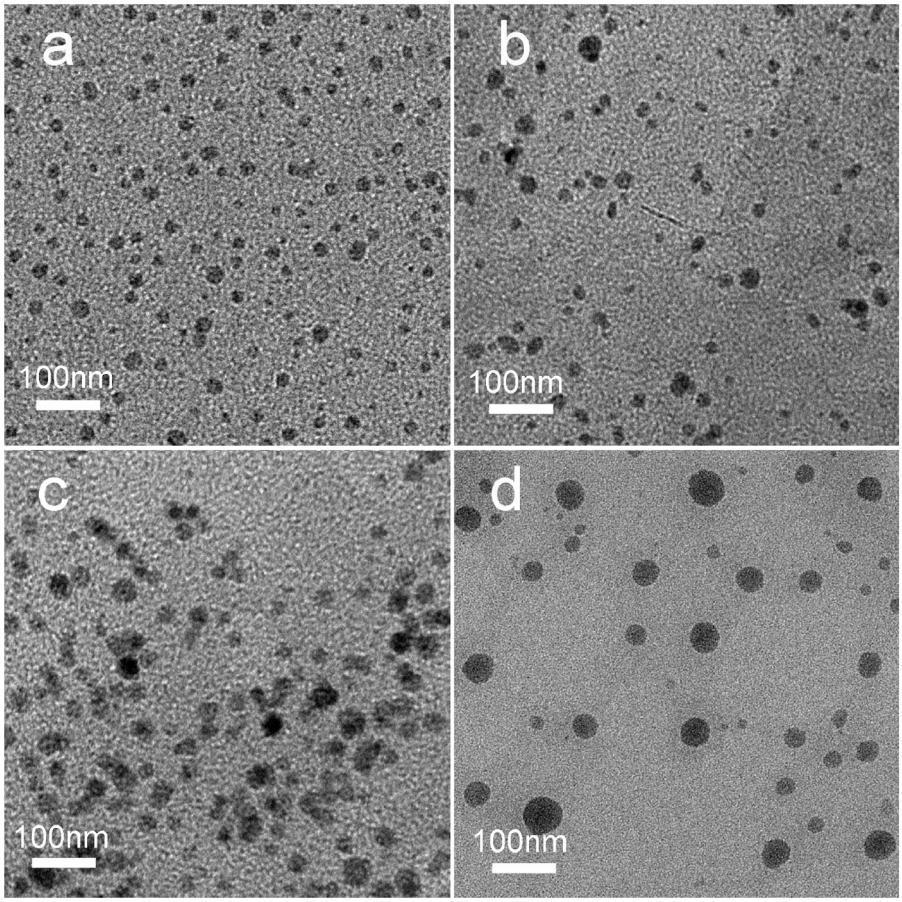

Fig. 2. TEM images of AgNPs synthesized with different amount of silver in the CNs/AgNPs nanocomposites (a) 0.36, (b) 1.77, (c) 3.47 and (d) 6.71 wt%.

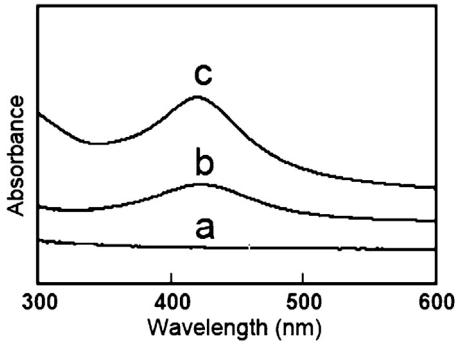

Fig. 4. UV–vis spectra of (a) PVA/CNs, (b) PVA/CNs/AgNPs, and (c) CNs/AgNPs.

The optical UV–vis absorption spectra of PVA/CNs, CNs/AgNPs-3.47, and PVA/CNs/AgNPs-3.47 films are shown in Fig. 4. UV–vis absorption spectra of PVA/CNs films did not show any peaks in the region of 300–600 nm (Fig. 4a), while PVA/CNs/AgNPs-3.47 film with the addition of silver nanoparticles resulted in the formation of a peak centered at 450 nm (Fig. 4c). It is well known that AgNPs exhibit a surface plasmon resonance band between 350 and 500 nm, and this is clearly evident for CNs/AgNPs-3.47 in Fig. 4b, and this band confirms the formation of silver nanoparticles within the polymer matrix. Surface plasmon resonance band of PVA/CNs/AgNPs is attributed to the presence of AgNPs. Compared with PVA/CNs/AgNPs, CNs/AgNPs shows no band shift due to surface plasmon resonance. It is a sign of the well-dispersed AgNPs within PVA matrices otherwise band shift will be caused by AgNPs' aggregation (Zhang, Roll, Geddes, & Lakowicz, 2004). The samples for XRD and UV–vis test by random selection throughout the matrix also imply that the CNs/AgNPs nanoparticles were distributed uniformly within the PVA polymer matrix.

3.3. Mechanical properties

The mechanical properties (tensile strength σ_B and elongation at break ε) of PVA films and composite films reinforced with various compositions of CNs and CNs/AgNPs nanocomposites were investigated by tensile testing at room temperature. Results of σ_B and ε are presented in Table 1 and Fig. 5 as a function of CNs and AgNP content for the PVA matrix composite films. Clearly, tensile strength was improved from 57.02 to 75.20 MPa, while elongation at break dereased from 391.47 to 340.61% upon increasing CNs content from 0 to 5 wt% PVA. This indicates that incorporating CNs into the PVA matrix results in strong interactions between the filler and matrix and, thus, restricts the matrix motion. Tensile strength and elongation at break of composite films change only slightly with a small amount of AgNPs (PVA/CNs/AgNPs-0.36) in Fig. 5. When the content of AgNPs increases to 1.77 wt%, tensile strength was improved from 75.20 to 81.21 MPa, while elongation at break dereased from 340.61 to 230.71%. However, tensile strength reduced with the increasing of the content of AgNPs, and elongation at break increased slightly. This phenomenon may be caused by coordination bonds of AgNPs with CNs and PVA, which can improve the intermolecular force.

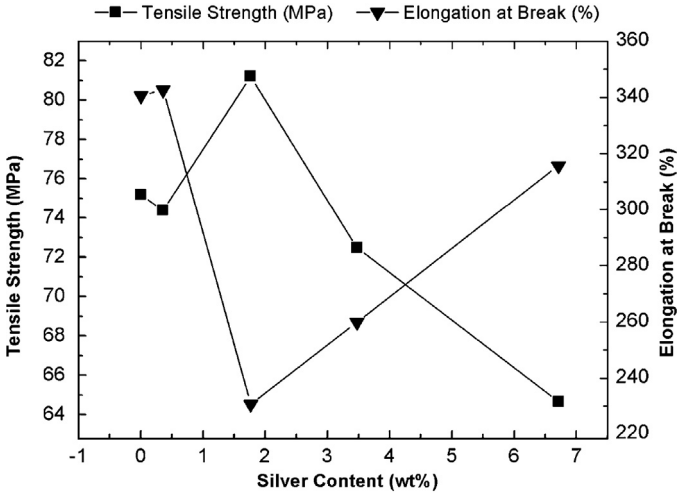

Fig. 5. Tensile strength and elongation at break for PVA-based films of different compositions.

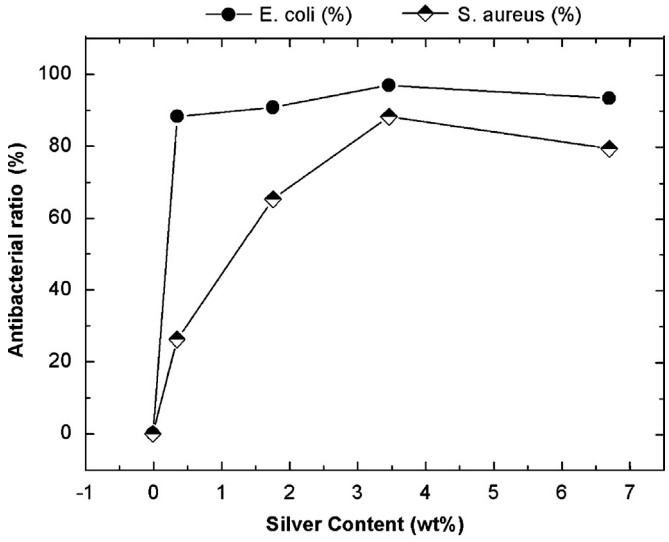

Fig. 6. Antibacterial activity of PVA/CNs/AgNPs composites to *E. coli* and *S. aureus*.

At the same time, the introduction of the AgNPs may enhance crystallinity of PVA (Huang, Wilkes, & Carlson, 1989; Hsu, Chou, & Tseng, 2004). That's why tensile strength of composite films is improved. But the excess AgNPs would break the interaction between the PVA matrix and the CNs and reduce tensile strength of the composite.

3.4. Antibacterial activity of PVA/CNs/AgNPs composites

The antibacterial activity of the pure PVA, PVA/CNs film and PVA/CNs/AgNPs composite films with various silver contents was tested using *E. coli* and *S. aureus* in Table 1 and Fig. 6. The PVA and

Table 1
Data showing of PVA-based films: tensile strength (σ_B), Elongation at break (ε), and Antibacterial ratio.

Sample	σ_B (MPa)	ε (%)	Antibacterial ratio of *E. coli* (%)	Antibacterial ratio of *S. aureus* (%)
PVA	57.02	391.47	0.0	0.0
PVA/CNs	75.20	340.61	0.0	0.0
PVA/CNs/AgNPs-0.36	74.39	342.66	88.3	26.2
PVA/CNs/AgNPs-1.77	81.21	230.71	90.8	65.3
PVA/CNs/AgNPs-3.47	72.48	259.88	96.9	88.2
PVA/CNs/AgNPs-6.71	64.67	315.66	93.3	79.3

PVA/CNs films show no antibacterial properties to both bacteria. All PVA/CNs/AgNPs composite films have strong and uniformed antibacterial activities to *E. coli*, but weaker antibacterial activities to *S. aureus*. A fluctuation in antibacterial activity has been observed with varying silver contents. The antibacterial activities have been enhanced by increasing the content of AgNPs to 3.47% (sample PVA/CNs/AgNPs-3.47), after that, the antibacterial performance is lowered by increasing the content of Ag nanoparticles from 3.47 to 6.71%. Antibacterial mechanisms of silver nanoparticles remain unresolved but it is commonly believed that AgNPs interact with constituents of bacteria's outer membrane, causing structural changes and degradation that eventually lead to cell death (Sondi & Salopek-Sondi, 2004; Morones et al., 2005). AgNPs with a size less than 15 nm are well-known to have efficient antibacterial activity because they are able to penetrate inside the bacteria and cause further damages, possibly by interacting with sulfur- and phosphorus-containing moieties of DNA (Sondi & Salopek-Sondi, 2004; Morones et al., 2005). It is conjectured that antibacterial activities of PVA/CNs/AgNPs result from altering the size of AgNPs by varying silver cation content in the synthesis process. Fig. 2 indicates that the nano-particles size increases with increasing silver cation content from 0.36 to 3.47 wt% (Fig. 2a and c), but size of AgNPs is still less than 15 nm. The increasing silver content will increase the amount or the total surface area of AgNPs, which result in the improvement of PVA-based composites' antibacterial activity. When silver cation content is saturated, most particles become much larger than 15 nm (Fig. 2d). Larger AgNPs would be unable to penetrate inside the bacteria, and thus reduce the antibacterial activity.

4. Conclusion

CNs/AgNP nanocomposites were prepared, and the morphology, the mechanical behavior, and the antibacterial activity of PVA-based composites and neat PVA were investigated. XRD and UV–vis results indicate that CNs and AgNPs are dispersed homogeneously within the PVA matrix. However, AgNPs and CNs show opposite effect on mechanical behavior. Tensile strength and elongation at break of composite films change only slightly with a small amount of AgNPs. But the excess AgNPs would break the interaction between the PVA matrix and the CNs and reduce tensile strength of the composite. More importantly, PVA/CNs/AgNPs composite films indicate a strong antibacterial activity against *E. coli* and *S. aureus*. The results indicate that CNs/AgNPs nanocomposites as reinforcing and antibacterial nanofiller are valuable for the PVA applications.

Acknowledgments

We gratefully acknowledge the financial support from the National Science and Technology Support Program (Grant 2012BAD32B05), and Project Funded by the Priority Academic Program Development of Jiangsu Higher Education Institutions.

References

Allen, N. S., Edge, M., Ortega, A., Sandoval, G., Liauw, C. M., Verran, J., Stratton, J., & McIntyre, R. B. (2004). Degradation and stabilisation of polymers and coatings: nano versus pigmentary titania particles. *Polymer Degradation and Stability*, *85*, 927–946.

Althues, H., Henle, J., & Kaskel, S. (2007). Functional inorganic nanofillers for transparent polymers. *Chemical Society Reviews*, *36*, 1454–1465.

Anglès, M. N., & Dufresne, A. (2011). Plasticized starch/tunicin whiskers nanocomposite materials 2. mechanical behavior. *Marcomolecules*, *34*, 2921–2931.

Bönnemann, H., & Richards, R. M. (2011). Nanoscopic metal particles-synthetic methods and potential applications. *European Journal of Inorganic Chemistry*, *10*, 2455–2480.

Brinchi, L., Cotana, F., Fortunati, E., & Kenny, J. M. (2013). Production of nanocrystalline cellulose from lignocellulosic biomass: Technology and applications. *Carbohydrate Polymers*, *94*, 154–169.

Cai, J., Kimura, S., Wada, M., & Kuga, S. (2009). Nanoporous cellulose as metal nanoparticles support. *Biomacromolecules*, *10*, 87–94.

Cao, X., Habibi, Y., & Lucia, L. A. (2009). One-pot polymerization, surface grafting and processing of waterborne polyurethane-cellulose nanocrystal nanocomposites. *Journal of Materials Chemistry*, *19*, 7137–7145.

Chen, D., Lawton, D., Thompson, M. R., & Liu, Q. (2012). Biocomposites reinforced with cellulose nanocrystals derived from potato peel waste. *Carbohydrate Polymers*, *1*, 709–716.

Clemons, C., Sedlmair, J., Illman, B., Ibach, R., & Hirschmugl, C. (2013). Chemically imaging the effects of the addition of nanofibrillated cellulose on the distribution of poly(acrylic acid) in poly(vinyl alcohol). *Polymer*, *54*, 2058–2061.

Eichhorn, S. J., Young, R. J., & Davies, G. R. (2005). Modeling crystal and molecular deformation in regenerated cellulose fibers. *Biomacromolecules*, *6*, 507–513.

Fortunati, E., Armentano, I., Zhou, Q., Iannoni, A., Saino, E., Visai, L., Berglund, L. A., & Kenny, J. M. (2012). Multifunctional bionanocomposite films of poly(lactic acid) cellulose nanocrystals and silver nanoparticles. *Carbohydrate Polymers*, *87*, 1596–1605.

Habibi, Y., & Dufresne, A. (2008). Highly filled bionanocomposites from functionalized polysaccharide nanocrystals. *Biomacromolecules*, *9*, 1974–1980.

Habibi, Y., Lucia, L. A., & Rojas, O. J. (2010). Cellulose nanocrystals: chemistry, self-assembly and applications. *Chemical Reviews*, *110*, 3479–3500.

Hsu, S. H., Chou, C. W., & Tseng, S. M. (2004). Enhanced thermal and mechanical properties in polyurethane/Au nanocomposites. *Macromolecular Materials and Engineering*, *289*, 1096–1101.

Huang, H. H., Wilkes, G. L., & Carlson, J. G. (1989). Structure-property behaviour of hybrid materials incorporating tetraethoxysilane with multifunctional poly (tetramethylene oxide). *Polymer*, *30*, 2001–2012.

Khan, A., Khan, R. A., Salmieri, S., Tien, C. L., Riedl, B., Bouchard, J., Chauve, G., Tan, V., Kamal, M. R., & Lacroix, M. (2012). Mechanical and barrier properties of nanocrystalline cellulose reinforced chitosan based nanocomposite films. *Carbohydrate Polymers*, *90*, 1601–1608.

Klemm, D., Heublein, B., Fink, H. P., & Bohn, A. (2005). Cellulose: Fascinating biopolymer and sustainable raw material. *Angewandte Chemie International Edition*, *44*, 3358–3393.

Kumar, A., Vemula, P. K., Ajayan, P. M., & John, G. (2008). Silver-nanoparticle-embedded antimicrobial paints based on vegetable oil. *Nature Materials*, *7*, 236–241.

Liu, H., Cui, S., Shang, S., Wang, D., & Song, J. (2013). Properties of rosin-based waterborne polyurethanes/cellulose nanocrystals composites. *Carbohydrate Polymers*, *96*, 510–515.

Liu, H., Wang, D., Shang, S., & Song, Z. (2011). Synthesis and characterization of Ag–Pd alloy nanoparticles/carboxylated cellulose nanocrystals nanocomposites. *Carbohydrate Polymers*, *83*, 38–43.

Ma, X. Y., & Zhang, W. D. (2009). Effects of flower-like ZnO nanowhiskers on the mechanical thermal and antibacterial properties of waterborne polyurethane. *Polymer Degradation and Stability*, *94*, 1103–1109.

De Menezes, A. J., Siqueira, G., Curvelo, A. A. S., & Dufresne, A. (2009). Extrusion and characterization of functionalized cellulose whisker reinforced polyethylene nanocomposites. *Polymer*, *50*, 4552–4563.

Morones, J. R., Elechiguerra, J. L., Camacho, A., Holt, K., Kouri, J. B., Ramírez, J. T., & Yacaman, M. J. (2005). The bactericidal effect of silver nanoparticles. *Nanotechnology*, *16*, 2346–2353.

Nathalie, L., Isabelle, D., Alain, D., & Julien, B. (2012). Microfibrillated cellulose-Its barrier properties and applications in cellulosic materials: A review. *Carbohydrate Polymers*, *90*, 735–764.

Parisa, P., Tae, K., Karl, J., Rina, T., & Hamid, G. (2013). Design of a cellulose-based nanocomposite as a potential polymeric scaffold in tissue engineering. *Polymer*, *54*, 2105–2114.

Shin, Y., Bae, I., Arey, B. W., & Exarhos, G. J. (2008). Facile stabilization of gold–silver alloy nanoparticles on cellulose nanocrystal. *Journal of Physical Chemistry C*, *112*, 4844–4848.

Shinsuke, I., Manami, T., Minoru, M., Hiroyuki, S., & Hiroyuki, Y. (2009). Synthesis of silver nanoparticles templated by TEMPO-mediated oxidized bacterial cellulose nanofibers. *Biomacromolecules*, *10*, 2714–2717.

Sondi, I., & Salopek-Sondi, B. (2004). Silver nanoparticles as antimicrobial agent: a case study on *E. coli* as a model for Gram-negative bacteria. *Journal of Colloid and Interface Science*, *275*, 177–182.

Ten, E., Jiang, L., & Wolcott, M. P. (2013). Preparation and properties of aligned poly(3-hydroxybutyrate-co-3-hydroxyvalerate)/cellulose nanowhiskers composites. *Carbohydrate Polymers*, *92*, 206–213.

Varga, Z., Feher, J., Filipcsei, G., & Zrinyi, M. (2003). Smart nanocomposite polymer gels. *Macromolecular Symposia*, *200*, 93–100.

Zhang, J., Roll, D., Geddes, C. D., & Lakowicz, J. R. (2004). Aggregation of silver nanoparticle-dextran adducts with concanavalin A and competitive complexation with glucose. *Journal of Physical Chemistry B*, *108*, 12210–12214.